Applied Surface Science Advances 27 (2025) 100765

Contents lists available at ScienceDirect

Applied Surface Science Advances

journal homepage: www.sciencedirect.com/journal/applied-surface-science-advances

Full Length Article

Pristine and cross-linked gelatin aerogels of pH-responsive hydration and swelling

Attila Forgács [a,*], Madalina Ranga [a], Andreea Ranga [a], László István Orosz [a], Geo Paul [b], Leonardo Marchese [b], Dániel Pércsi [a,c], Adél Len [c,f], Zoltán Dudás [c], Gergő Vecsei [d], Attila Csík [e], István Fábián [a], József Kalmár [a]

[a] HUN-REN-DE Mechanisms of Complex Homogeneous and Heterogeneous Chemical Reactions Research Group, Department of Inorganic and Analytical Chemistry, University of Debrecen, Egyetem tér 1, Debrecen H-4032, Hungary
[b] Department of Science and Technological Innovation, Universitá del Piemonte Orientale, Viale T. Michel 11, Alessandria 15121, Italy
[c] HUN-REN Centre for Energy Research, Budapest Neutron Centre, Konkoly-Thege M. str. 29-33, Budapest H-1121, Hungary
[d] Department of Solid State Physics, Faculty of Science and Technology, University of Debrecen, P.O. Box 400, Debrecen H-4002, Hungary
[e] HUN-REN Institute for Nuclear Research, Bem tér 18/C, Debrecen H-4026, Hungary
[f] Faculty of Engineering and Information Technology, University of Pécs, Boszorkány str. 2, Pécs H-7624, Hungary

ARTICLE INFO

Keywords:
Aerogel
Sustainable
Drug delivery
gelatin
pH responsive

ABSTRACT

Protein aerogels, derived from natural sources such as plants and animals, are sustainable and biocompatible advanced materials with significant potential for applications in the environmental, food, and pharmaceutical industries. In this study, food-grade gelatin was used to produce highly porous aerogels. Gelatin was employed either in its native form or chemically cross-linked with glutaraldehyde (GTA). Hydrogels were synthesized through a simple sol-gel process, transferred to methanol, and then dried using supercritical CO_2 to obtain mesoporous aerogels. The chemical structure of the aerogels was characterized using solid-state nuclear magnetic resonance (ssNMR) and infrared (IR) spectroscopy methods. Their nanoscale morphologies were explored by scanning electron microscopy (SEM), N_2-sorption porosimetry, and small-angle neutron scattering (SANS). The macroscopic water uptake and swelling of the gelatin aerogels were investigated at different pH values, while the corresponding nanoscale hydration and wetting mechanisms were explored using NMR relaxometry. Lastly, the drug loratadine was impregnated into the pure gelatin aerogel to assess its potential for drug delivery applications. The rate and mechanism of in vitro drug release exhibit a strong correlation with the pH-dependent swelling and dissolution of the aerogel. These findings suggest that pure gelatin aerogels are promising candidates for pH-sensitive oral drug delivery systems.

1. Introduction

Aerogels represent a distinctive class of porous materials in which gas replaces the liquid component within the pores without altering the structure of the material. Over the past decade, interest in aerogels has grown significantly due to their remarkable and unique properties. These highly porous, lightweight materials are characterized by low density, high surface area, and exceptional low thermal and electrical conductivities [1,2] Typically, aerogels consist of a network of interconnected nanoparticles or nanofibers, forming a complex three-dimensional architecture. One of the latest research directions involves the use of aerogels as drug delivery systems [3–6] The application of aerogels as host matrices for biomaterials has expanded significantly in recent years [3,5,7–9] Supercritically dried aerogels provide promising platforms for drug delivery, particularly in oral and pulmonary applications [10–12] Their advantageous hydration properties make them highly effective for drug delivery, with biopolymer aerogels emerging as one of the most significant subcategories [5–7,13]

Importantly, aerogels can be formulated from biomaterials that are already used in pharmaceutical technology [14,15] The field of biopolymer aerogels is rapidly expanding, attracting significant scientific interest due to their advantages over traditional synthetic polymers. Derived from natural and renewable sources, such as plants and animal tissues, biopolymer aerogels are sustainable advanced materials. They

* Corresponding author.
E-mail address: forgacs.attila@science.unideb.hu (A. Forgács).

https://doi.org/10.1016/j.apsadv.2025.100765
Received 10 February 2025; Received in revised form 2 May 2025; Accepted 3 May 2025
Available online 9 May 2025

are biocompatible and safe for use in the pharmaceutical and food industries [16,17] Biopolymer aerogels can effectively be impregnated with active compounds through adsorptive precipitation using supercritical CO_2, a method that retains the active ingredient in an amorphous state within the porous system [18–21] From a therapeutic perspective, controlling the release kinetics is crucial for optimizing drug delivery efficacy, whether by accelerating or slowing down drug release [22]

Mehling et al. demonstrated the effectiveness of drug loading and release from starch and alginate aerogels, showing promising results for delivering drugs such as paracetamol and ibuprofen [23] Their findings revealed that aerogels made from certain types of biopolymers with higher porosity enabled faster drug release, highlighting their potential for responsive delivery systems. Kéri et al. investigated the release of ketoprofen and ibuprofen from silica-gelatin aerogels, demonstrating that the gelatin content significantly influenced drug release from the pore system [18] Loratadine is classified in the international Biopharmaceutical Classification System (BCS) as a class II drug, meaning that it displays poor water solubility, but rapid biosorption. The bioavailability of such drugs largely depends on their release rate from the formulation. One approach to increasing solubility is loading the drug into a porous carrier [24–27] Lovskaya et al. studied the impregnation of loratadine into alginate-based aerogels, achieving >20 % drug loading [28] Stability tests indicated that the amorphous loratadine content remained stable, suggesting that alginate-based aerogels are suitable carriers.

Gelatin is a biopolymer obtained through the thermal denaturation of collagen, a natural protein of animal origin. It consists of long, flexible polypeptide chains that form coils and loops, held together by hydrogen bonds and hydrophobic forces in a three-dimensional network [29,30] This structure enables gelatin to form stable solvated gels with water and other protic solvents, such as alcohols. Due to its excellent biocompatibility, biodegradability, and non-immunogenicity, gelatin is widely used as a natural macromolecule in biomedicine [31–33] Furthermore, extracting gelatin from agricultural waste plays a crucial role in maximizing the utilization of animal byproducts, contributing to a zero-waste food economy [34,35] The amino acid chains in gelatin can undergo crosslinking reactions with aldehydes that modify its gelling properties and introduce new physical characteristics, such as enhanced durability, thermal stability, water insolubility, and altered chemical reactivity [36–38] Glutaraldehyde is commonly used as a crosslinker for proteins and polypeptides, particularly gelatin, due to its ability to form stable covalent bonds with amino groups. This process enhances protein stability and functionality for various applications [39,40]

This study explores newly synthesized aerogels composed entirely of natural gelatin, as well as, glutaraldehyde (GTA) cross-linked gelatin. These supercritically dried, high-porosity gelatin aerogels have never been investigated as pH-responsive drug delivery systems. The aerogels were characterized using various techniques, including SEM, N_2-porosimetry, IR spectroscopy, SANS, NMR relaxometry, solid-state NMR, water uptake measurements, and compressive strength testing. The pristine gelatin aerogel was loaded with the model active ingredient loratadine, and its release behavior was investigated as a function of pH. Finally, the drug release profiles were correlated with the aerogel's pH-dependent water uptake and swelling properties.

2. Materials and methods

2.1. Materials and solutions

The gelatin used in this study was obtained as food-grade gelatin sheets from Dr. Oetker. It is type A gelatin derived from porcine sources, with a mean molecular weight of 150 kDa and a Bloom strength of 240. Its consistent quality control and high purity make it suitable for research purposes. Glutaraldehyde (GTA) and HPLC-grade methanol were purchased from Sigma Aldrich. Aqueous solutions were prepared using ultra-filtered, double-deionized water (Elga PureLab Classic system). Supercritical CO_2 was prepared from 99.5+% purity gas from Linde. Ph.Eur. grade loratadine from Cadila Healthcare Limited was used for the experiments.

2.2. Preparation of pristine gelatin aerogels

Gelatin aerogels were prepared using the sol-gel method. Gelatin sheets were cut into small pieces, and the required amount (Table 1) was dissolved in 25 mL of water at 60–70 °C. The dissolution process was carried out under stirring at 50 rpm for 15 min, followed by an increase to 150 rpm for an additional 10 min. Once the gelatin was fully dissolved, the mixture was allowed to cool to room temperature while being continuously stirred at 300 rpm. The resulting mixture was then poured into cylindrical plastic molds, sealed airtight, and aged in a refrigerator at 4 °C for 16 h.

2.3. Preparation of cross-linked gelatin aerogels

The required amount of gelatin (Table 1) was dissolved in 20 mL of water as described in the previous section. Various concentrations of GTA solutions were prepared by dissolving solid GTA (Table 1) in 5 mL of water. The two solutions were then mixed at room temperature and stirred at high rate for 20 to 45 s to ensure homogenization. Finally, the mixture was quickly poured into molds, sealed, and refrigerated at 4 °C for 16 h.

For both the pristine and the cross-linked gelatins, the preparation was followed in the same way. First, a three-step solvent exchange was performed to replace water with methanol in the gels. To remove the residual water from the porous structure, a continuous-mode solvent regeneration and extraction distillation unit was used. Finally, methanol was extracted using supercritical CO_2 at 100 bar and 40 °C to obtain aerogels [41]

The aerogels were coded based on their gelatin and GTA content in the gelation mixtures, as indicated in Table 1. The total volume of each reaction mixture was consistently maintained at 25 mL.

Images of the as-prepared aerogel monoliths are provided in **Figure S1** in the **Supplementary Information (SI)**. The preparation of the presented aerogels are highly reproducible and scalable. **Table S1** in the **SI** shows the structural characteristics of samples from different batches prepared ca. 8 months apart.

2.4. Characterization methods

The infrared (FT-IR) spectra of the samples were recorded using a PerkinElmer Spectrum IR-ES instrument. Data analysis was performed with Spectrum IR-ES version 10.7.2.1630 (PerkinElmer). Spectra were taken at a resolution of 2 cm^{-1}, with an accumulation of 8 scans.

Solid-state NMR spectra were acquired on a Bruker Avance III 500 spectrometer equipped with a wide bore 11.75 T magnet, operating at frequencies of 500.13 MHz for ^{1}H and 125.77 MHz for ^{13}C. A 4 mm triple-resonance probe in double-resonance mode with magic angle spinning (MAS) was used in all experiments. For optimal sensitivity, the rotor was fitted with Teflon inserts, defining a volume of 50 µL. The

Table 1
Codes of the prepared aerogels and their composition.

Code	Gelatin amount (g)	GTA amount (g)
RM.03.000	3.0	–
RM.04.000	4.0	–
RM.06.000	6.0	–
RM.03.010	3.0	0.10
RM.04.010	4.0	0.10
RM.04.025	4.0	0.25
RM.04.050	4.0	0.50
RM.04.075	4.0	0.75
RM.03.100	3.0	1.0
RM.04.100	4.0	1.0

samples were packed into a zirconia rotor and spun at a MAS rate between 10 and 15 kHz. The radio frequency (RF) field strength was 100 kHz for ^{1}H NMR. For the ^{13}C cross polarization (CP) MAS experiments, RF fields of 55 and 28 kHz were used for initial proton excitation and decoupling, respectively. During the CP period, the ^{1}H RF field was ramped using 100 increments, while the ^{13}C RF field was kept constant. During acquisition, proton decoupling from carbon was achieved using a two-pulse phase-modulated (TPPM) decoupling scheme. A moderate ramped RF field of 62 kHz was used for spin-locking, while the carbon RF field was adjusted for optimal signal. The relaxation delay between accumulations was 5 s and the CP contact time was 2 ms. All chemical shifts are reported on the δ scale externally referenced to tetramethylsilane (TMS) at 0 ppm.

The morphology of the aerogels was examined by scanning electron microscopy (SEM) using a ThermoFisher Scientific Scios 2 instrument. The as-prepared aerogels were gently fractured, and the freshly fractured inner surface of the aerogels were imaged by SEM. No sample pretreatment was applied. The samples were fixed onto vacuum-resistant carbon tape. A low acceleration voltage (1–2 kV) was applied to minimize charging effects on the aerogels, eliminating the need for sputter coating.

Small-angle neutron scattering (SANS) measurements were performed using the Yellow Submarine instrument at the Budapest Neutron Center (BNC), which is a pinhole-type instrument equipped with a two-dimensional neutron detector [13,42] Two sample-to-detector distances (1.2 m and 5.3 m) and two neutron wavelengths (4.15 Å and 9.70 Å) were used, covering a Q range of 0.010 – 0.446 Å^{-1}. The measured scattering intensity was corrected for sample transmission, empty cell scattering, detector sensitivity, and background scattering. The structural parameters of the scattering objects were determined through mathematical analysis of the corrected intensity versus scattering vector ($I(Q)$) curves. For a broad Q range, where both Guinier and Porod approximations apply to the different sections of the SANS curve, a combined approach was used known as the Beaucage model [43] Data fitting was performed using the non-linear Levenberg-Marquardt least-squares algorithm in the open-source software SasView 5.0.4. Additional details on the measurement setup and data evaluation are provided in the **SI**.

The apparent specific surface area, pore size distribution, and total pore volume were measured by N_2-sorption porosimetry with a Quantachrome Nova 2200e instrument. The as-prepared aerogels were gently cut into sub-millimeter sized pieces, and degassed in vacuum at 40 °C for 24 h before starting the addition of N_2 for the sorption measurements. Data analysis was performed using NovaWin 11.0 software (Quantachrome Instruments, USA). The specific surface area was calculated using the multipoint BET method, while the pore size distribution was derived from the desorption curves using the BJH method. The NLDFT method was not applied due to the absence of a suitable kernel for the gelatin backbone.

Compression tests were carried out using an Instron instrument at room temperature, with a crosshead speed of 1 mm•min^{-1} and a full-scale load range of 10 kN. Cylindrical aerogel monoliths (diameter: 15 mm, height: 22 mm) were prepared, and the tests were performed in triplicates. Data was recorded using Instron Series IX Automated Materials Tester v.8.30.00 software. Young's modulus was determined by the software.

The water uptake of the aerogels was monitored over 72 h at four pH values (1.0, 2.0, 7.0, and 8.0) adjusted with HCl and NaOH. These pH values were chosen to obtain information on the behavior of the aerogels covering the whole pH range relevant to natural body fluids. Cylindrical samples (diameter: 15 mm, height: 5.0 mm) were weighed and measured every 30 min. Changes in size were recorded using a vernier caliper, and mass was measured with an analytical balance. To assess the effect of sample size on water uptake, smaller aerogel pieces (diameter: 3.0 mm, height: 2.0 mm) were also tested. The changes in the mass and the volume of the monolithic aerogel samples were recorded. The water uptake ratio (WUR) was determined using the following formula.

$$WUR = \frac{W_w - W_d}{W_d} \quad (1)$$

Here, W_w is the mass of the wet aerogel, and W_d is the mass of the dry aerogel. By measuring changes in height and diameter, the volume change was calculated. For the small (3 mm diameter) samples, only the mass change was determined.

NMR relaxometry experiments were conducted using a 20 MHz Minispec Bruker mq20 relaxometer, employing the classical CPMG (Carr-Purcell-Meiboom-Gill) spin-echo pulse sequence. Experiments were performed on samples hydrated in multiple steps. For all T_2 measurements, the CPMG sequence was applied using three echo times (0.08 ms, 0.12 ms, and 0.16 ms), with parameters optimized based on T_1 relaxation times determined earlier using the inversion–recovery method. The water-to-dry aerogel mass ratio was increased from 0 to 2.5 g/g in 16 incremental steps. Approximately 50 mg of dry aerogel was weighed into a relaxometric tube and titrated with water. The wet aerogel samples were mixed, sonicated, and stored in a refrigerator for 24 h to ensure complete equilibration before NMR measurements. One sample (RM.04.000) was titrated with a pH = 2.5 HCl solution. In this case, measurement settings remained the same, except that the hydration liquid was different.

2.5. Impregnation and release of loratadine

The drug loratadine (Scheme 1) was impregnated into the RM.03.000 pure gelatin aerogel in supercritical CO_2 by adsorptive precipitation [5,21] This is an advanced technique for loading poorly water soluble drugs into hydrophilic porous carrier matrices. This technique ensures both the conservation of the high porosity of the carrier, and the amorphization of the drug even at high drug contents. These features are otherwise inaccessible by other impregnation strategies, as highlighted in the literature [5,21]

The aerogel (45 mg) was ground and wrapped in filter paper. Loratadine (90 mg) was also wrapped in filter paper and placed in the same autoclave as the aerogel. This setup ensured that only dissolved loratadine could come into physical contact with the aerogel.

The autoclave containing the wrapped components was filled with supercritical CO_2 at 110 bar and 40 °C, and the system was equilibrated under these conditions for 16 h. Finally, the autoclave was depressurized at ca. 1 bar/min. The impregnated aerogel was carefully removed from the filter paper wrapping and analyzed.

Powder XRD measurements were conducted to assess the crystallinity of the deposited loratadine in the aerogel, as detailed in the **SI**.

To determine the active pharmaceutical ingredient (pure loratadine) content, the loaded aerogel samples were dispersed in methanol, sonicated in a water bath at 25 °C for 15 min, and further agitated for 8 h. The loratadine concentration in the solution was determined using

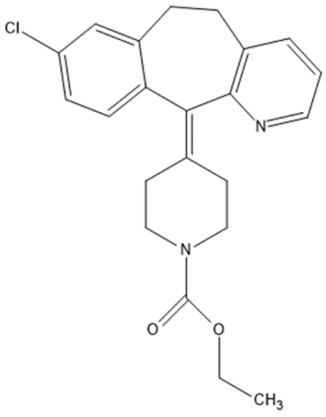

Scheme 1. Chemical structure of loratadine.

HPLC. A Phenomenex Kinetex C8 column was used at 40 °C under isocratic conditions, with a 4 μL injection volume and a 5 min runtime. The mobile phase consisted of a water-to-methanol ratio of 15:85, with a flow rate of 0.5 mL/min. UV–vis detection was performed in the wavelength range of 210–400 nm.

Drug release kinetic curves were recorded using a customized fast kinetics method with on-line UV–vis spectrophotometric detection, as described in details in earlier publications [4,18] Briefly, a specified amount (0.50 – 1.50 mg) of loaded aerogel was weighed into a dry standard quartz cuvette (1.0 cm × 1.0 cm). Spectrophotometric detection was started, and 3.0 mL of the release medium was injected into the cuvette. UV–vis spectra were recorded in every 5 s. The system was continuously stirred using a magnetic stir bar at 200 rpm, while the temperature was maintained at 37 °C. The concentration of the released nicotinic acid was calculated from the on-line measured absorbance values based on a series of external calibration solutions [44] Drug release experiments were conducted in two media: pH = 2.5 HCl solution, and pH = 7.4 phosphate buffered saline (PBS). These are the generally applied pharmacopeia media for drug release tests simulating the gastric fluid, and the intestinal fluid, respectively.

3. Results and discussion

3.1. FT-IR spectroscopy

The characteristic IR bands of polypeptides were identified in the spectra of both the pristine and the cross-linked gelatin aerogels (Fig. 1) [45–47] The assignments of the most significant bands are as follows: 3275–3295 cm^{-1} for amide N—H bending, 2900–3000 cm^{-1} for C—H stretching, 1590–1690 cm^{-1} for N—H stretching, 1406–1438 cm^{-1} for C—H bending, and 1215–1337 cm^{-1} for C—N stretching. However, no distinct peaks corresponding to GTA reaction products were observed due to overlap with the high-intensity peaks originating from gelatin. According to the literature, glutaraldehyde cross-linking of polypeptides typically produces detectable peaks only at much higher GTA-to-peptide ratios [39,40] A comparison of the various samples revealed no significant differences in the IR spectra, regardless of the gelatin content, or the amount of the cross-linking agent used. The IR spectra of gelatin and GTA are compared with those of the pristine and cross-linked aerogels in **Figure S2** in the **SI**.

Although the IR spectra did not directly confirm successful cross-linking, the observed color change in the prepared monoliths (see **Figure S1** in the **SI**), along with the morphological alterations identified through SEM imaging and N_2 porosimetry (vide infra), suggest that cross-linking was achieved. Furthermore, the significant differences in compressive strength among the aerogels, as well as their distinct behaviors in water uptake experiments (vide infra) provide additional evidence supporting the success of the cross-linking process.

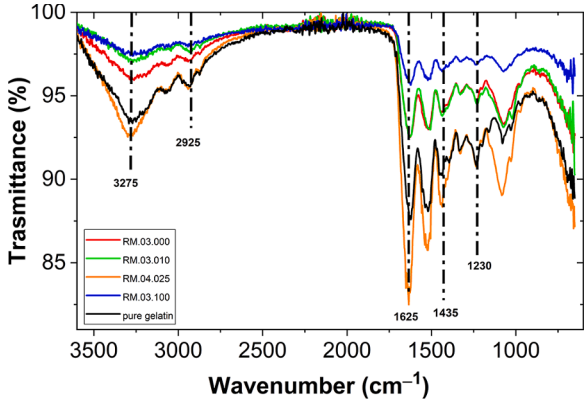

Fig. 1. Infrared spectra of the gelatin aerogels, and that of the raw material gelatin.

3.2. Solid state NMR

The ^{13}C CPMAS and ^{1}H MAS NMR spectra of gelatin (RM.04.000, RM.03.000) and cross-linked gelatin (RM.03.010, RM.04.010) aerogels are shown in Fig. 2. In the ^{13}C CPMAS spectra, the broad resonance between δ = 155–180 ppm is attributed to carbonyl carbon atoms in gelatin. The narrower peaks within 15–70 ppm can be attributed to specific amino acids. This includes glycine (Gly) at 42.7 ppm, the most abundant amino acid in gelatin; proline (Pro) at 24.9 ppm and 47.3 ppm; glutamic acid (Glu) at 29.5 ppm and 54.3 ppm; alanine (Ala) at 47.3 ppm; and hydroxyproline (Hyp) at 54.3 ppm and 70.5 ppm. Small peaks at 120–140 ppm are assigned to aromatic carbons, and the peak at δ = 157.0 ppm corresponds to arginine (Arg). The carbonyl region (163 to 184 ppm) shows peaks for the carboxylic amino acid side chains in gelatin [48] The cross-linking between gelatin and GTA were not detected in the ^{13}C CPMAS NMR spectra due to the overlapping of carbon peaks in the carbonyl region. However, the ^{1}H-MAS NMR spectra showed notable changes between pure gelatin and GTA cross-linked gelatin aerogels. The proton peak associated to –NH, –OH groups and H_2O at 4.6 ppm displayed a narrowing effect upon GTA cross-linking. Furthermore, the very broad peak in the down-field region at 7–12 ppm due to hydrogen-bonding protons, showed a decrease in intensity upon GTA cross-linking [49] Essentially, these NMR features confirm the partial breakage of the hydrogen-bonding network and the molecular-level reorganization of the 3D structure of gelatin upon cross-linking.

3.3. Scanning electron microscopy (SEM)

Characteristic SEM images of pristine and cross-linked gelatin aerogels (Fig. 3 and **Figure S3** in the **SI**) reveal a homogeneous, quasi-fibrous morphology with smooth surfaces, free of ridges and cracks. No significant morphological differences are observed between the pristine and the cross-linked gelatin aerogels, as both exhibit a dense architecture with visible pores in 50 000 × magnification in the SEM images. Although, the N_2-sorption measurements revealed differences between the pore structures of the pristine and the cross-linked gelatin aerogels, as discussed in the next section.

3.4. N_2 adsorption-desorption porosimetry

Representative N_2 adsorption-desorption isotherms of pristine and cross-linked gelatin aerogels are shown in Fig. 4. Additional N_2-sorption isotherms, pore size distribution curves and structural data are given in the **SI** (**Figure S4** and **Table S2**) for supporting the following discussion.

All hysteresis curves correspond to IUPAC category IV with an H2b-type loop, which is characteristic of mesoporous materials [50] This isotherm type indicates a mesoporous structure with pore diameters primarily ranging from 2 to 30 nm, featuring mixed-shaped pores, and the presence of some macropores. However, these larger pores that are also visible in the SEM images in 50 000 × magnification, cannot be filled by condensed N_2 during measurement.

A morphological difference is observed when comparing cross-linked aerogels to pristine ones. The hysteresis loops of pristine samples resemble more of the H1 type, indicating cylindrical pores, whereas the H2b feature in the isotherms becomes more pronounced with increasing concentrations of the cross-linking agent. Additionally, cross-linked gelatin aerogels exhibit a narrower pore size distribution. Mean pore sizes and total pore volumes are summarized in Table 2, although these parameters are strongly influenced by the presence of macropores that cannot be filled by condensed N_2.

Apparent specific surface areas, determined by the BET method, are significantly higher for pristine gelatin aerogels and decrease as the cross-linking agent concentration increases. A similar trend is observed

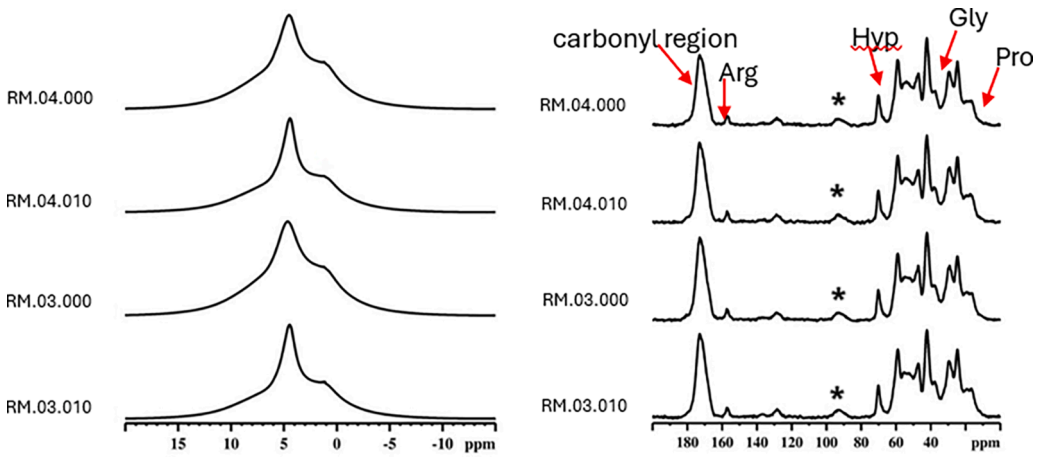

Fig. 2. ^{1}H MAS (left panel) and ^{13}C CPMAS (right panel) NMR spectra of pristine gelatin and cross-linked gelatin aerogels. A MAS rate of 15 and 10 kHz were used for ^{1}H MAS and ^{13}C CPMAS NMR experiments, respectively. * Spinning sidebands.

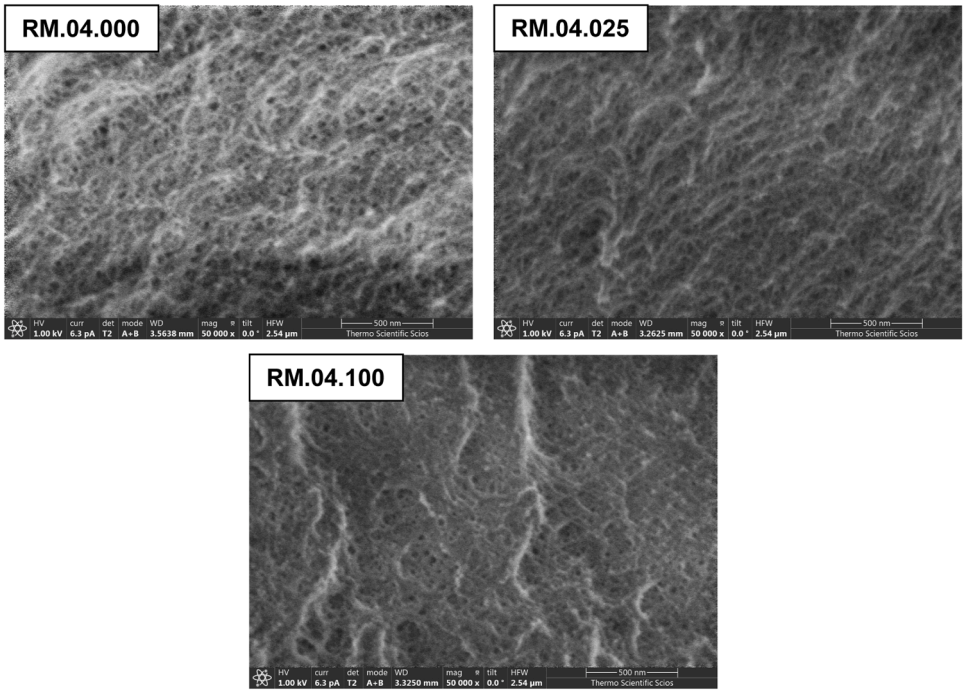

Fig. 3. SEM images of pristine gelatin and cross-linked gelatin aerogels in 50 000 × magnification. The scale bars represent 500 nm. (Additional images are shown in the **SI**.).

in pore diameter (Fig. 4). Pristine gelatin aerogels maintain a slightly higher apparent surface area until a cross-linking agent concentration of 0.25 g GTA in 5 mL water (RM.04.025), beyond which the surface area steadily decreases with further cross-linking.

3.5. SANS measurements

Representative experimental scattering curves together with the best fits with the Beaucage model are shown in Fig. 5. The estimated structural parameters are summarized in Table 3. Additional SANS curves are shown in the **SI** (**Figure S5**).

A comparison of the SANS curves reveals no significant morphological differences between the pristine and cross-linked gelatin aerogels. This indicates that the nanometer-sized primary structural units of the aerogels are practically identical across all materials, regardless of the gelatin content or the presence and concentration of the cross-linking agent. As shown in Table 3, the R_g and p values are nearly identical in all cases. Assuming that the R_g values correspond to the pore sizes in this mesoporous material, the estimated pore diameter ranges from 34 to 40 nm [51] These sizes align well with observations from the SEM images, the N_2-sorption results, and the descriptions of similar gelatin aerogels in the literature [29,52–55]

Kratky plots were also constructed for each sample. The average diameter of the primary nanofibers corresponds to the position of the intensity maximum (Q_{max}) on these plots, which is nearly identical across all aerogels (Fig. 5). This indicates that the size of the primary nanofibers is consistent in all the aerogels [56] However, as mentioned previously, the spatial arrangement of these primary fibers must differ to explain the observed variations in porosity and pore size distribution, as measured by N_2-sorption.

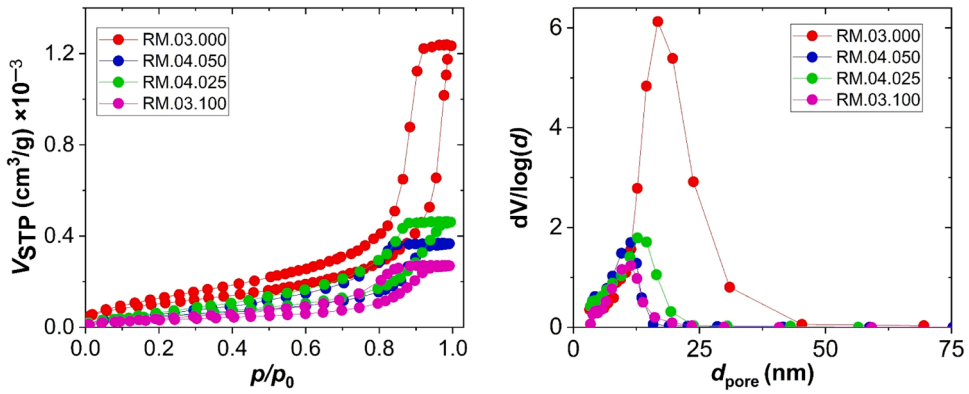

Fig. 4. Left panel: Nitrogen adsorption-desorption isotherms of the aerogels given in the legend. Right panel: Pore size distribution curves calculated from the desorption isotherms using the BJH method. (Additional data is given in the **SI**.).

Table 2
Structural parameters of the aerogels estimated by the BET and the BJH methods from N_2 adsorption-desorption porosimetry.

	RM.03.000	RM.04.050	RM.04.025	RM.03.100	Data evaluation
Specific surface area (m^2 g^{-1})	567	319	353	220	BET
Mean pore size (nm)	17 ± 1	11 ± 2	13 ± 2	9.6 ± 2	BJH
Total pore volume (cm^3 g^{-1})	1.9	0.59	0.73	0.44	BJH

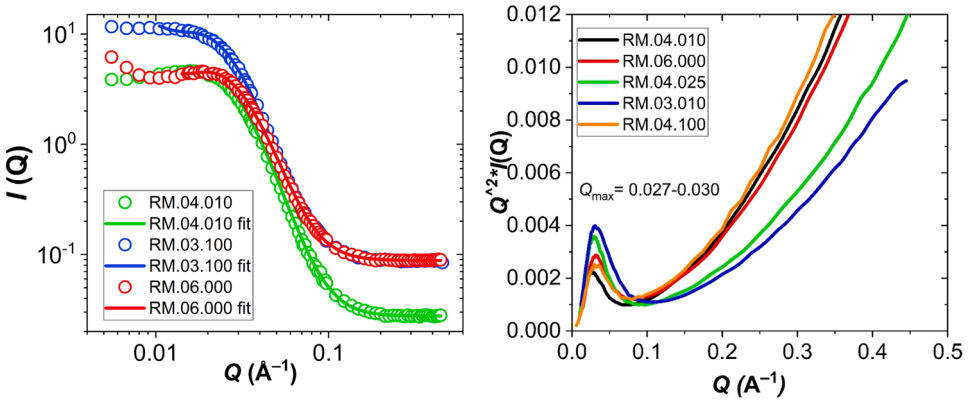

Fig. 5. Left: The experimental SANS curves (markers) together with the best fits (lines) of the Beaucage model. Right: Kratky plots calculated from the scattering curves.

Table 3
Calculated properties derived from the SANS measurements using the Beaucage model, and the X^2 value describing the goodness of the fit.

Sample	R_g (A)	d_{pore} (nm)	p	X^2
RM.04.010	153	39.6	4.12	1.33
RM.06.000	131	33.8	4.33	1.88
RM.03.010	130	33.6	4.17	3.79
RM.04.100	133	34.5	4.11	3.19
RM.03.100	152	39.2	4.44	3.73
RM.04.000	134	34.6	4.09	1.97

3.6. Compressive strength

Experimental strain-stress curves are shown in Fig. 6. The corresponding Young's modulus values, calculated using the classical methods by the instrument software, are listed in Table 4.

The monolithic aerogels exhibit three typical stages of deformation under compressive stress: elastic deformation, compaction, and densification [57] While few compressive strength measurements have been made on bulk gelatin aerogels, previously studied monoliths have shown significantly improved mechanical properties when incorporated into composite materials [58–60]

Photographs of the monolithic aerogels, taken before and after compression (Fig. 7), reveal no surface cracks, indicating that the material is homogeneous at the macroscopic level. These aerogels display impressive mechanical properties and behave similarly to plastics, making them promising for load-bearing applications, which is beyond the scope of this article. In summary, the gelatin aerogels exhibit substantially higher compressive strength compared to most conventional inorganic and organic aerogels [61]

Young's modulus increases monotonously with the amount of cross-linking agent, suggesting that the chemical cross-linking process successfully strengthened the gelatin network.

3.7. Water uptake of aerogels

Water uptake measurements are essential for evaluating the potential of bio-based materials in specific biomedical applications, as swelling and dissolution in aqueous environments are key factors

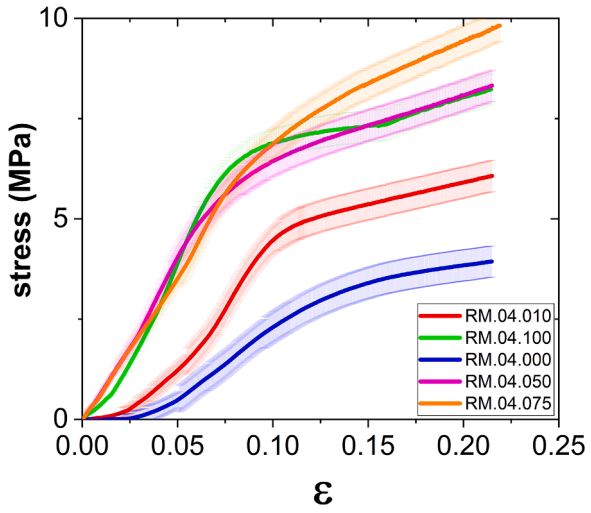

Fig. 6. Representative compressive strain-stress curves characterizing the pristine gelatin and the cross-linked gelatin aerogels. The error bars represent the standard deviation calculated from triplicate measurements using independent samples.

Table 4
Young's modulus values of pristine gelatin and cross-linked gelatin aerogels.

RM.04.000	RM.04.010	RM.04.050	RM.04.075	RM.04.100
37 ± 1 MPa	61 ± 1 MPa	86 ± 2 MPa	84 ± 2 MPa	107 ± 2 MPa

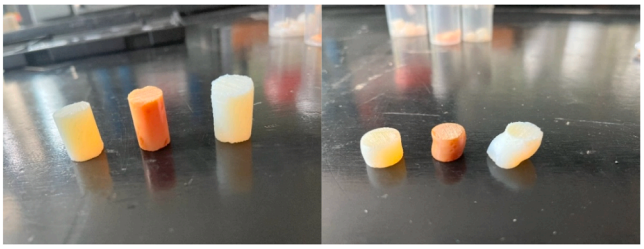

Fig. 7. Aerogel monoliths before and after the compression tests.

influencing material performance [62–64]

The highest water uptake and swelling were observed in the non-crosslinked gelatin aerogel (RM.03.000), while the lowest water uptake occurred in the sample with the highest cross-linker content (RM.04.100), as shown in Figs. 8 and 9. Naturally, reduced swelling and water uptake are expected when introducing chemical cross-links into an inherently hydrophilic biopolymer.

When comparing the effects in different media, the highest volume change and water uptake were observed under acidic conditions, followed by neutral and basic pH. At pH = 1.0, even the cross-linked aerogels dissolved within approximately 5 h.

Additionally, during the water uptake experiments, the aerogels' yellowish color gradually became transparent. This visual change occurred most rapidly under acidic conditions, suggesting that the bonds between the gelatin and the cross-linking agent hydrolyze over time.

Comparing hydration rates between small aerogel pieces and larger discs revealed that the hydration rate is practically independent of sample size. This indicates that the chemical structure of the gelatin backbone and its morphology are the primary factors influencing the hydration and swelling rates of the aerogel monoliths, rather than their macroscopic size.

3.8. NMR relaxometry measurements

The structural characteristics of hydrated aerogels were investigated using NMR relaxometry technique. Generally, NMR relaxometry is an indirect method for the exploration of water localization in different chemical environments within the nanoscale structure of the hydrated aerogels [13] The T_2 value reflects the interactions between water molecules and the solid backbones of the aerogels. The change of the T_2 values provides insights into the hydration and wetting mechanism. Already established considerations were used to draw mechanistic conclusions [13,51,65,66]

The RM.06.000, RM.04.000, and RM.04.010 aerogels were titrated with water stepwise, up to a maximum water-to-aerogel ratio of 2.5 g/g. At each step, the T_2 values (spin-spin relaxation times of water protons) were measured. For titration with an HCl solution, the procedure was the same, but the titration was stopped at a maximum water-to-aerogel ratio of 1.4 g/g.

Overall, the relaxation data for water titration showed minimal variation among the pure gelatin and cross-linked gelatin aerogels, regardless of the gelatin content or the amount of cross-linking agent used. All hydrated aerogels exhibited three distinct relaxation domains, as shown in Fig. 10. The first domain starts at the lowest water content, the second at 0.2–0.3 g/g, followed by the third around 0.5 g/g.

The first relaxation domain, with the lowest T_2 values (from 0.5 to 8.0 ms), consists of water molecules that are tightly bound to the gelatin macromolecules. These water molecules are strongly associated with the gelatin skeleton, specifically merging into the primary nanoscale fibers. This water can be considered structural, as it is strongly connected to the macromolecular framework. The measured T_2 values increase up to a water content of 1.5 g/g, after which they level off.

The second domain, with intermediate T_2 relaxation times, corresponds to the primary, highly ordered hydration shell on the nanoscale skeleton. In this domain, water molecules form a structured layer on the surface of the nanofibers, creating a primary hydration shell around the solid framework. This domain behaves similarly to the first, reaching a plateau around a water content of 1.5 g/g.

The third domain, with the highest T_2 values, corresponds to water in small droplets or puddles confined within the entangled nanofiber network. These T_2 values are characteristic of water molecules that move relatively freely within the pores. As the water content increases, the T_2 values steadily increase, reflecting decreasing molecular constraints as the pores fill and quasi-bulk phases form.

When comparing the amplitudes of the three domains, they generally follow the same trend as the T_2 values. The first and second domains are challenging to distinguish mathematically, but they can be separated using the MERA algorithm for inverse Laplace transformation [67] This is partly due to their smaller amplitudes compared to the third domain. Additionally, the amplitudes of the first two domains reach a maximum with increasing water content, while the third domain increases linearly (**Figure S6** in the **SI**). These results suggest that water exchange occurs between the first two domains, while the third domain remains well-separated even at high water content.

The RM.04.000 sample was also titrated with an HCl solution (pH = 2.5). The titration was halted at a water-to-aerogel ratio of 1.4 g/g, as the sample began to dissolve at this point. The results, shown in Fig. 11, were compared with those obtained using water. Notably, only two relaxation domains were observed during the HCl titration, as opposed to the three observed when titrating with water. The first two relaxation domains, associated with strongly bound water, merged under acidic conditions, while the third domain, associated with larger puddles, behaved similarly in both cases. The merging of the first two domains is attributed to the fast exchange of water between the structural water and the hydration sphere in the acidic medium, likely due to partial dissolution of the gelatin backbone. This behavior aligns with the water uptake measurements (Section 3.8), where the pristine gelatin aerogels swell dramatically and take up large amounts of water under acidic

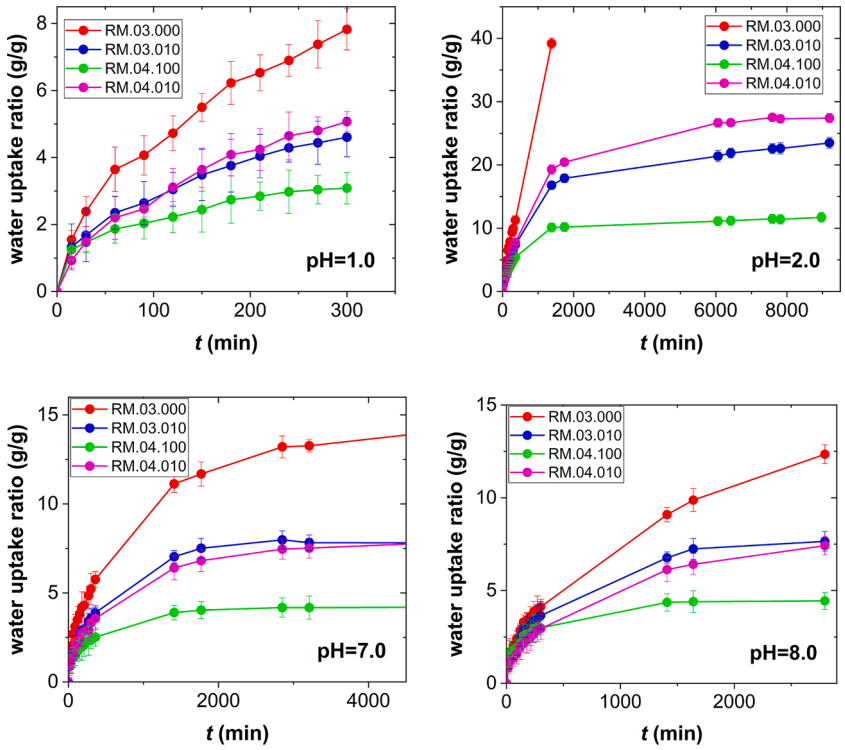

Fig. 8. Water uptake of monolithic aerogels over time at different pH values. The error bars represent the standard deviation calculated from triplicate measurements.

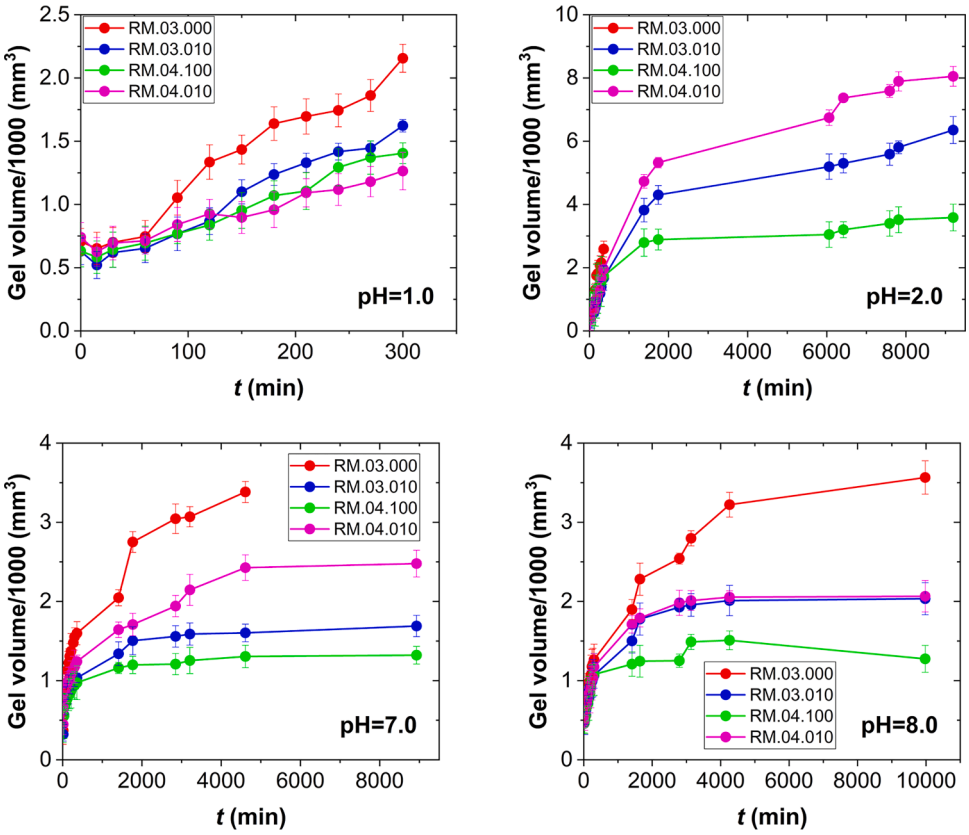

Fig. 9. Volume change of monolithic aerogels over time at different pH values. The error bars represent the standard deviation calculated from triplicate measurements.

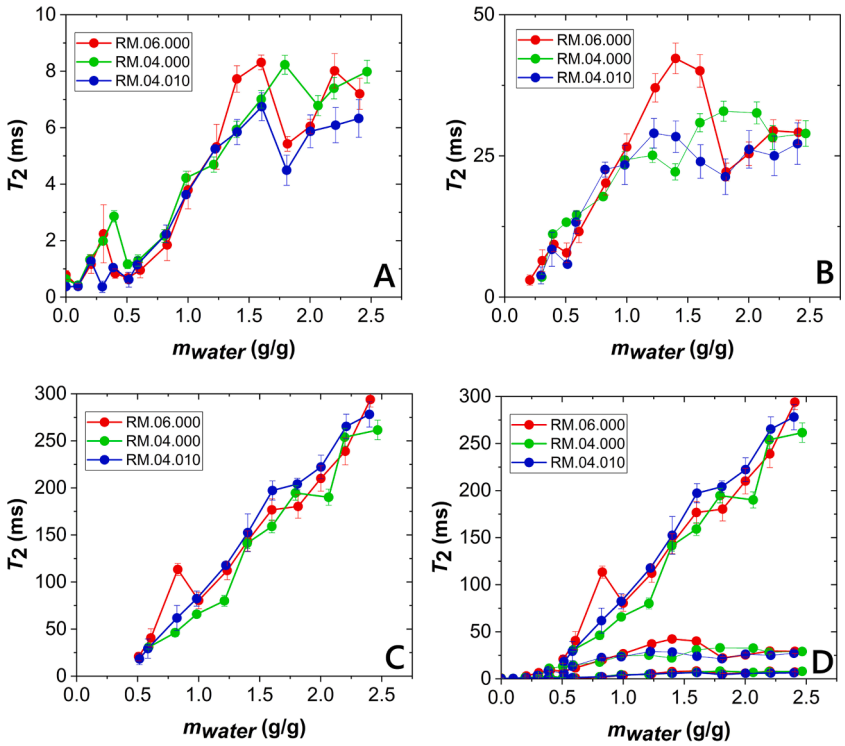

Fig. 10. Measured T_2 relaxation times as function of water content given in grams of water per grams of dry aerogel. Panels A, B, C show the first, second and third domains, respectively, and panel D shows all three domains together. The error bars represent the standard deviation calculated from triplicate measurements.

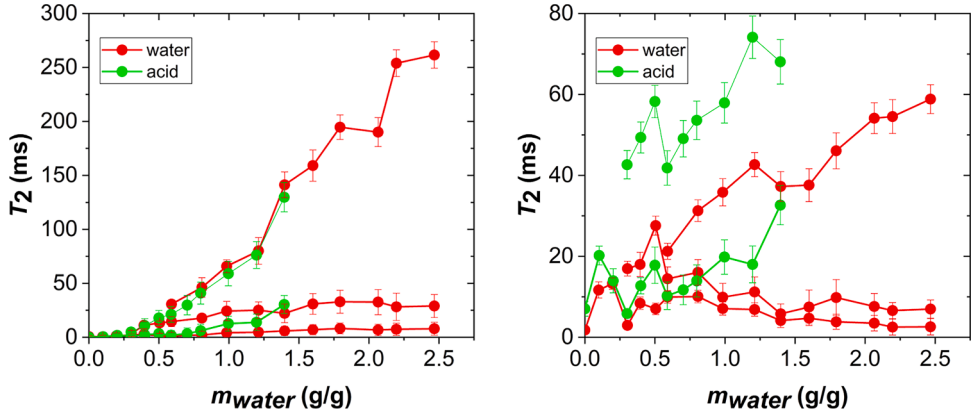

Fig. 11. Left panel: The T_2 relaxation times as the function of water content of the RM.04.000 aerogel measured using pure water (red markers) or a pH = 2.5 HCl solution (green markers). Right panel: The corresponding amplitudes of the relaxation domains. The error bars represent the standard deviation calculated from triplicate measurements.

conditions, reflecting the extensive hydration of the gelatin skeleton as seen in the NMR relaxometry results.

3.9. Impregnation and release of loratadine

Loratadine was impregnated into the RM.03.000 pristine gelatin aerogel using the technique of adsorptive deposition in supercritical CO_2 [14] The process was designed to approximate the pure loratadine content of solid drug formulations available on the market. The loaded aerogel contains 1.7 w/w% pure loratadine, which is close to the content found in market-standard formulations, such as the Loratadine-Ratiopharm 10 mg tablets (EU market).

Powder XRD measurements indicated that the pristine aerogel is amorphous, and the deposited loratadine does not crystallize in the loaded aerogel formulations. (XRD diffractograms are provided in **Figure S7** in the **SI**.) The amorphous nature of loratadine plays a crucial role in determining its release profile.

The dissolution of pure loratadine and its release from the loaded aerogel were investigated in HCl solution at pH = 2.5 and in PBS at pH = 7.4. In both media, the amount of pure loratadine in the dissolution cell was set to 95 % of its solubility limit at the respective pH. The solubility of loratadine is 0.09 mg/ml at pH = 2.5 and 0.004 mg/ml at pH = 7.4 [68]

Drug release from the loaded aerogel differs significantly from the dissolution of pure loratadine in both media, as shown in Fig. 12. At pH = 2.5, the dissolution of pure loratadine occurs in two phases: an initial rapid phase followed by a slower phase as its concentration approaches the solubility limit. In contrast, the release of amorphous loratadine from the aerogel follows a single kinetic phase, even near its solubility limit. The timeframes for both the dissolution of pure loratadine and the

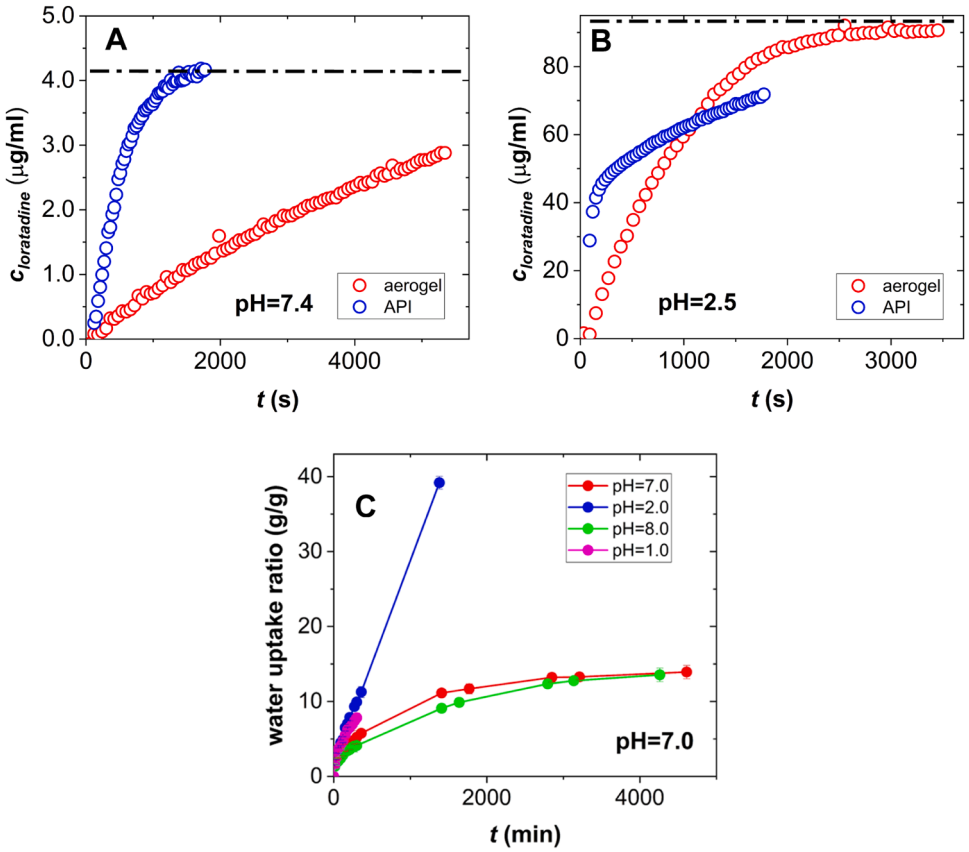

Fig. 12. The dissolution of pure loratadine (API), and the release of the loaded loratadine from the aerogel at pH = 7.4 in PBS (A) and at pH = 2.5 in HCl (B). The data points in panel A and B are the average of duplicate measurements. The relative deviation between the duplicates is <10 %. Panel C: Water uptake of the as-prepared RM.03.000 gelatin aerogel in different media. The error bars in panel C represent the standard deviation calculated from triplicate measurements.

drug release from the aerogel are approximately the same. While the solubility of loratadine is extremely limited in PBS, its dissolution rate is as fast as in HCl, whereas its release from the loaded aerogel is significantly slower under these conditions.

Under the applied conditions, the dissolution of loratadine is primarily limited by its solubility. However, when encapsulated within the aerogel's pore structure, its dissolution is also influenced by the structure of the aerogel skeleton. The water uptake of the RM.03.000 gelatin aerogel is significantly slower at pH = 7.4 compared to acidic conditions, proceeding at roughly half the rate (cf. Fig. 8). This behavior is clearly reflected in the drug release at different pH values. For comparison, the pH dependence of the water uptake of the related cross-linked RM.03.010 aerogel is given in **Figure S8** in the **SI**. Evidently, the pristine gelatin aerogel is more sensitive to the pH than the cross-linked ones, and the high pH-sensitivity of the pristine gelatin aerogel is an advantageous feature for drug delivery applications, as follows.

Under acidic conditions, where the system is well-hydrated, the aerogel carrier has minimal impact on the rate of drug release compared to the dissolution of pure loratadine. In contrast, at pH = 7.4, where the system is poorly hydrated, the aerogel's encapsulating effect becomes more pronounced, slowing down the drug release compared to the dissolution of the pure drug.

The pK_a of protonated loratadine is 4.6, meaning that loratadine exists as a cation at pH = 2.5, but remains neutral at pH = 7.4 [27] Therefore, hydrophobic interactions between loratadine and the gelatin backbone can result in the strong binding of the pure loratadine to the carrier at pH = 7.4, which can also contribute to the retarded drug release [69]

Overall, the gelatin aerogel proved to be a versatile pH-sensitive drug delivery system. It effectively encapsulates the drug at near-neutral pH, delaying its release, while also serving as a solubilizing aid under acidic conditions. This dual functionality makes it highly suitable for oral drug delivery, where it can enhance the effective concentration of poorly water-soluble loratadine in gastric fluids.

Importantly, it has been demonstrated earlier that gelatin and gelatin-derived hybrid aerogels are biocompatible and non-toxic [4,15, 70–72]

4. Conclusions

Gelatin and cross-linked gelatin aerogels can be synthesized via the sol-gel method, even at high gelatin concentrations. Glutaraldehyde cross-links the gelatin during alcogel preparation, and supercritical CO_2 extraction yields high-porosity aerogels.

The aerogels' solid backbone consists of fibril-like structures, influencing mechanical strength and hydration properties. Nitrogen-sorption measurements confirmed mesoporosity, with apparent surface areas up to 600 m^2/g, and pore sizes of 10–30 nm. The aerogels exhibit high Young's modulus (35–105 MPa), increasing with cross-linker content.

Swelling and water uptake measurements were performed in the wide pH range from 1.0 to 8.0. The aerogels showed higher water absorption and faster swelling under acidic conditions. Furthermore, NMR relaxometry confirmed the enhanced hydration and partial dissolution of the gelatin backbone in acidic media.

Loratadine was incorporated into pure gelatin aerogel via adsorptive deposition in supercritical CO_2. Drug release studies were carried out at 37 °C in two media: pH = 2.5 HCl solution, and pH = 7.4 phosphate buffered saline (PBS). These are the generally applied pharmacopeia media for drug release tests simulating the gastric fluid, and the intestinal fluid, respectively. The drug release experiments showed that the

aerogel retards loratadine dissolution at neutral pH but enhances solubility in acidic conditions, making it suitable for pH-sensitive oral drug delivery.

APPENDIX: Supplementary material

The ***Supplementary Information (SI)*** related to this article can be found in the online version of the article. Additional experimental details are given on the characterization techniques, including the SANS and the XRD methods referred to in the text. Additional experimental results including SEM, N_2-sorption, SANS, XRD, NMR and water uptake data are given as referred to in the main text of the article.

CRediT authorship contribution statement

Attila Forgács: Writing – review & editing, Writing – original draft, Visualization, Validation, Supervision, Methodology, Formal analysis, Data curation, Conceptualization. **Madalina Ranga:** Formal analysis, Data curation. **Andreea Ranga:** Formal analysis, Data curation. **László István Orosz:** Formal analysis, Data curation. **Geo Paul:** Formal analysis, Data curation. **Leonardo Marchese:** Resources, Funding acquisition. **Dániel Pércsi:** Formal analysis, Data curation. **Adél Len:** Writing – review & editing, Formal analysis, Data curation. **Zoltán Dudás:** Writing – review & editing, Resources, Formal analysis, Data curation. **Gergő Vecsei:** Formal analysis, Data curation. **Attila Csík:** Formal analysis, Data curation. **István Fábián:** Writing – review & editing, Supervision, Resources, Funding acquisition. **József Kalmár:** Writing – review & editing, Writing – original draft, Validation, Supervision, Resources, Methodology, Funding acquisition, Formal analysis, Data curation.

Declaration of competing interest

The authors declare that they have no known competing financial interests or personal relationships that could have appeared to influence the work reported in this paper.

Acknowledgments

This research project has been financially supported by the National Research, Development and Innovation Fund of the Ministry of Culture and Innovation, Hungary (National Research, Development and Innovation Office, NKKP: SNN-150561) and the National Research, Development and Innovation Fund of the Ministry for Innovation and Technology, Hungary (project 2019–2.1.7-ERANET-2021–00021). This research was supported by the University of Debrecen Research Fund DETKA. J. Kalmár is grateful for the financial support of the János Bolyai Research Scholarship of the Hungarian Academy of Sciences.

Supplementary materials

Supplementary material associated with this article can be found, in the online version, at doi:10.1016/j.apsadv.2025.100765.

Data availability

Data will be made available on request.

References

[1] I. Smirnova, P. Gurikov, Aerogel production: current status, research directions, and future opportunities, J. Supercrit. Fluids. 134 (2018) 228–233.
[2] J. Stergar, U. Maver, Review of aerogel-based materials in biomedical applications, J. Solgel. Sci. Technol. 77 (2016) 738–752.
[3] Z. Ulker, C. Erkey, An emerging platform for drug delivery: aerogel based systems, J. Controll. Release 177 (2014) 51–63.
[4] P. Veres, M. Kéri, I. Bányai, I. Lázár, I. Fábián, C. Domingo, J. Kalmár, Mechanism of drug release from silica-gelatin aerogel—Relationship between matrix structure and release kinetics, Colloids Surfaces B. 152 (2017) 229–237.
[5] C.A. García-González, A. Sosnik, J. Kalmár, I. De Marco, C. Erkey, A. Concheiro, C. Alvarez-Lorenzo, Aerogels in drug delivery: from design to application, J. Controll. Release 332 (2021) 40–63.
[6] V.S. Gonçalves, P. Gurikov, J. Poejo, A.A. Matias, S. Heinrich, C.M. Duarte, I. Smirnova, Alginate-based hybrid aerogel microparticles for mucosal drug delivery, Europe. J. Pharm. Biopharm. 107 (2016) 160–170.
[7] C.A. García-González, M. Alnaief, I. Smirnova, Polysaccharide-based aerogels—Promising biodegradable carriers for drug delivery systems, Carbohydr. Polym. 86 (2011) 1425–1438.
[8] I. Smirnova, S. Suttiruengwong, W. Arlt, Feasibility study of hydrophilic and hydrophobic silica aerogels as drug delivery systems, J. Non Cryst. Solids. 350 (2004) 54–60.
[9] S. Wei, Y.C. Ching, C.H. Chuah, Synthesis of chitosan aerogels as promising carriers for drug delivery: a review, Carbohydr. Polym. 231 (2020) 115744.
[10] C. López-Iglesias, A.M. Casielles, A. Altay, R. Bettini, C. Alvarez-Lorenzo, C. A. García-González, From the printer to the lungs: inkjet-printed aerogel particles for pulmonary delivery, Chem. Eng. J. 357 (2019) 559–566.
[11] T. Athamneh, A. Amin, E. Benke, R. Ambrus, C.S. Leopold, P. Gurikov, I. Smirnova, Alginate and hybrid alginate-hyaluronic acid aerogel microspheres as potential carrier for pulmonary drug delivery, J. Supercrit. Fluids 150 (2019) 49–55.
[12] T.A. Esquivel-Castro, M. Ibarra-Alonso, J. Oliva, A. Martínez-Luévanos, Porous aerogel and core/shell nanoparticles for controlled drug delivery: a review, Mater. Sci. Eng. 96 (2019) 915–940.
[13] I. Lázár, A. Forgács, A. Horváth, G. Király, G. Nagy, A. Len, Z. Dudás, V. Papp, Z. Balogh, K. Moldován, Mechanism of hydration of biocompatible silica-casein aerogels probed by NMR and SANS reveal backbone rigidity, Appl. Surf. Sci. 531 (2020) 147232.
[14] I. Smirnova, C.A. García-González, P. Gurikov, Pharmaceutical applications of aerogels, Springer Handbook of Aerogels, Springer, 2023, pp. 1489–1504.
[15] G. Nagy, G. Király, P. Veres, I. Lázár, I. Fábián, G. Bánfalvi, I. Juhász, J. Kalmár, Controlled release of methotrexate from functionalized silica-gelatin aerogel microparticles applied against tumor cell growth, Int. J. Pharm. 558 (2019) 396–403.
[16] K.S. Mikkonen, K. Parikka, J.-P. Suuronen, A. Ghafar, R. Serimaa, M. Tenkanen, Enzymatic oxidation as a potential new route to produce polysaccharide aerogels, 4, Rsc Advances, 2014, pp. 11884–11892.
[17] N. Abhari, A. Madadlou, A. Dini, Structure of starch aerogel as affected by crosslinking and feasibility assessment of the aerogel for an anti-fungal volatile release, Food Chem. 221 (2017) 147–152.
[18] M. Kéri, A. Forgács, V. Papp, I. Bányai, P. Veres, A. Len, Z. Dudás, I. Fábián, J. Kalmár, Gelatin content governs hydration induced structural changes in silica-gelatin hybrid aerogels–Implications in drug delivery, Acta Biomater. 105 (2020) 131–145.
[19] M. Pantić, Ž. Knez, Z. Novak, Supercritical impregnation as a feasible technique for entrapment of fat-soluble vitamins into alginate aerogels, J. Non Cryst. Solids 432 (2016) 519–526.
[20] W. Li-Hong, C. Xin, X. Hui, Z. Li-Li, H. Jing, Z. Mei-Juan, L. Jie, L. Yi, L. Jin-Wen, Z. Wei, A novel strategy to design sustained-release poorly water-soluble drug mesoporous silica microparticles based on supercritical fluid technique, Int. J. Pharm. 454 (2013) 135–142.
[21] P. Gurikov, I. Smirnova, Amorphization of drugs by adsorptive precipitation from supercritical solutions: a review, J. Supercrit. Fluids 132 (2018) 105–125.
[22] T.A. Esquivel-Castro, G. Robledo-Trujillo, J. Oliva, H. Rosu, V. Rodríguez-González, A functional SiO2-TiO2 mesoporous assembly designed for the controlled release of carvacrol, Appl. Surface Sci. Adv. 13 (2023) 100378.
[23] T. Mehling, I. Smirnova, U. Guenther, R.H. Neubert, Polysaccharide-based aerogels as drug carriers, J. Non Cryst. Solids 355 (2009) 2472–2479.
[24] J. Han, B. Xiao, P.K. Le, C. Mangwandi, Enhancement of the solubility of BS class II drugs with MOF and MOF/GO composite materials: case studies of felodipine, ketoprofen and ibuprofen, Materials (Basel) 16 (2023) 1554.
[25] K. Jahan, Z. Sultana, S. Karim, H. Ali, J. Uddin, Enhancement of dissolution properties of poorly water soluble drug loratadineby using different techniques of solid dispersion, World J. Sci. Eng. 2 (2017) 103–108.
[26] J. Wang, R. Chang, Y. Zhao, J. Zhang, T. Zhang, Q. Fu, C. Chang, A. Zeng, Coamorphous loratadine-citric acid system with enhanced physical stability and bioavailability, Aaps. Pharmscitech. 18 (2017) 2541–2550.
[27] G. Popović, M. Čakar, D. Agbaba, Acid–base equilibria, solubilityof loratadine, desloratadinein water, micellar media, J. Pharm. Biomed. Anal. 49 (2009) 42–47.
[28] D. Lovskaya, N. Menshutina, Alginate-based aerogel particles as drug delivery systems: investigation of the supercritical adsorption and in vitro evaluations, Mater. 13 (2020) 329.
[29] D.n. Pércsi, A. Forgács, T. Fodor, I. Fábián, J. Kalmár, P. Herman, Nanostructured gelatin Aerogel for selective recovery of aqueous Pd (II) based on coordination to the peptide backbone, ACS Appl. Nano Mater. (2024).
[30] P. Herman, K. Moldován, G. Paul, L. Marchese, Z. Balogh, A. Len, Z. Dudás, I. Fábián, J. Kalmár, Selective and reversible surface complexation of aqueous palladium (II) by polycarboxylate (pyromellitic acid) functionalized hybrid aerogel sorbent, Appl. Surf. Sci. 613 (2023) 156026.
[31] K. Han, Q. Bai, W. Wu, N. Sun, N. Cui, T. Lu, Gelatin-based adhesive hydrogel with self-healing, hemostasis, and electrical conductivity, Int. J. Biol. Macromol. 183 (2021) 2142–2151.
[32] Q. Xing, K. Yates, C. Vogt, Z. Qian, M.C. Frost, F. Zhao, Increasing mechanical strength of gelatin hydrogels by divalent metal ion removal, Sci. Rep. 4 (2014) 4706.
[33] J.B. Rose, S. Pacelli, A.J. El Haj, H.S. Dua, A. Hopkinson, L.J. White, F.R. Rose, Gelatin-based mater. ocular tissue eng, Materials 7 (2014) 3106–3135.

[34] K. Su, C. Wang, Recent advances in the use of gelatin in biomedical research, Biotechnol. Lett. 37 (2015) 2139–2145.
[35] E.T.A. Tümerkan, Sustainable utilization of gelatin from animal-based Agri–food waste for the food industry and pharmacology, Valorization Agri-Food Wastes By-Products (2021) 425–442.
[36] A. Bigi, G. Cojazzi, S. Panzavolta, K. Rubini, N. Roveri, Mechanical and thermal properties of gelatin films at different degrees of glutaraldehyde crosslinking, Biomaterials 22 (2001) 763–768.
[37] E. Leo, M.A. Vandelli, R. Cameroni, F. Forni, Doxorubicin-loaded gelatin nanoparticles stabilized by glutaraldehyde: involvement of the drug in the cross-linking process, Int. J. Pharm. 155 (1997) 75–82.
[38] A. Talebian, S. Kordestani, A. Rashidi, F. Dadashian, M. Montazer, The effect of glutaraldehyde on the properties of gelatin films, Kem. Ind 56 (2007) 537–541.
[39] H.S. Mansur, C.M. Sadahira, A.N. Souza, A.A. Mansur, FTIR spectroscopy characterization of poly (vinyl alcohol) hydrogel with different hydrolysis degree and chemically crosslinked with glutaraldehyde, Mater. Sci. Eng. 28 (2008) 539–548.
[40] Y. You, X. Sun, Q. Cui, B. Wang, J. Ma, The retention and drainage behavior of cross-linked gelatin with glutaraldehyde in a papermaking system, BioResources 11 (3) (2016) 6162–6173.
[41] I. Lázár, I. Fábián, A continuous extraction and pumpless supercritical CO2 drying system for laboratory-scale aerogel production, Gels 2 (2016) 26.
[42] L. Almásy, New measurement control software on the Yellow Submarine SANS instrument at the Budapest Neutron Centre, J. Surface Invest. 15 (2021) 527–531.
[43] B. Hammouda, Analysis of the Beaucage model, J. Appl. Crystallogr. 43 (2010) 1474–1478.
[44] A. Liu, W. Lin, S. Ping, W. Guan, N. Hu, S. Zheng, Y. Ren, Analysis of degradation and pathways of three common antihistamine drugs by NaClO, UV, and UV-NaClO methods, Environ. Sci. Pollut. Res. 29 (2022) 43984–44002.
[45] T. Ahmad, A. Ismail, S.A. Ahmad, K.Abdul Khalil, E.A. Awad, M.T. Akhtar, A. Q. Sazili, Recovery of gelatin from bovine skin with the aid of pepsin and its effects on the characteristics of the extracted gelatin, Polymers 13 (2021) 1554.
[46] S.R. Derkach, Y.A. Kuchina, D.S. Kolotova, N.G. Voron'ko, Polyelectrolyte polysaccharide–gelatin complexes: rheology and structure, Polymers 12 (2020) 266.
[47] C. Hermida-Merino, D. Cabaleiro, L. Lugo, J. Valcarcel, J.A. Vázquez, I. Bravo, A. Longo, G. Salloum-Abou-Jaoude, E. Solano, C. Gracia-Fernández, Characterization of tuna gelatin-based hydrogels as a matrix for drug delivery, Gels 8 (2022) 237.
[48] S.F. Soares, S. Fateixa, T. Trindade, A.L. Daniel-da-Silva, A versatile synthetic route towards gelatin-silica hybrids and magnetic composite colloidal nanoparticles, Adv. Compos. Hybrid. Mater. 5 (2022) 884–898.
[49] G. Paul, S. Steuernagel, H. Koller, Non-covalent interactions of a drug molecule encapsulated in a hybrid silica gelelectronic supplementary information (ESI) available, Experimental details and additional figures, See, 2007.
[50] M. Thommes, K. Kaneko, A.V. Neimark, J.P. Olivier, F. Rodriguez-Reinoso, J. Rouquerol, K.S.W. Sing, Physisorption of gases, with special reference to the evaluation of surface area and pore size distribution (IUPAC Technical Report), Pure Appl. Chem. 87 (2015) 1051–1069.
[51] A. Forgács, V. Papp, G. Paul, L. Marchese, A. Len, Z. Dudás, I. Fábián, P. Gurikov, J. Kalmár, Mechanism of hydration and hydration induced structural changes of calcium alginate aerogel, ACS Appl. Mater. Interfaces. 13 (2021) 2997–3010.
[52] L. Yun, J. Zhao, X. Kang, Y. Du, X. Yuan, X. Hou, Preparation and properties of monolithic and hydrophobic gelatin–silica composite aerogels for oil absorption, J. Solgel. Sci. Technol. 83 (2017) 197–206.
[53] J. Wang, D. Zhao, K. Shang, Y.-T. Wang, D.-D. Ye, A.-H. Kang, W. Liao, Y.-Z. Wang, Ultrasoft gelatin aerogels for oil contaminant removal, J. Mater. Chem. A. 4 (2016) 9381–9389.
[54] T. Pan, X. Cui, Gelatin aerogel with good mechanical properties and adjustable physical properties for boron adsorption from salt lake brines: an optimized process, Int. J. Biol. Macromol. 251 (2023) 126403.
[55] J. Jiang, Q. Zhang, X. Zhan, F. Chen, A multifunctional gelatin-based aerogel with superior pollutants adsorption, oil/water separation and photocatalytic properties, Chem. Eng. J. 358 (2019) 1539–1551.
[56] P. Veres, D. Sebők, I. Dékány, P. Gurikov, I. Smirnova, I. Fábián, J. Kalmár, A redox strategy to tailor the release properties of Fe (III)-alginate aerogels for oral drug delivery, Carbohydr. Polym. 188 (2018) 159–167.
[57] B. Fu, H. Luo, F. Wang, G. Churu, K. Chu, J.C. Hanan, C. Sotiriou-Leventis, N. Leventis, H. Lu, Simulation of the microstructural evolution of a polymer crosslinked templated silica aerogel under high-strain-rate compression, J. Non Cryst. Solids 357 (2011) 2063–2074.
[58] H. Li, F. Zhao, T. Peng, C. Jiang, H. Liu, Y. He, D. He, Robust, lightweight gelatin composite aerogel with outstanding thermal insulation, J. Mater. Sci. 57 (2022) 14835–14847.
[59] M. Sachithanadam, S.C. Joshi, High strain recovery with improved mechanical properties of gelatin–silica aerogel composites post-binding treatment, J. Mater. Sci. 49 (2014) 163–179.
[60] J. Zhu, F. Zhao, R. Xiong, T. Peng, Y. Ma, J. Hu, L. Xie, C. Jiang, Thermal insulation and flame retardancy of attapulgite reinforced gelatin-based composite aerogel with enhanced strength properties, Composites Part A. 138 (2020) 106040.
[61] K.A. Obrey, K.V. Wilson, D.A. Loy, Enhancing mechanical properties of silica aerogels, J. Non Cryst. Solids 357 (2011) 3435–3441.
[62] E. Effraimopoulou, J. Kalmár, G. Paul, L. Marchese, D. Ioannou, P. Paraskevopoulou, P. Gurikov, Whey protein isolate-based aerogels with improved hydration properties for food packaging applications, ACS Appl. Nano Mater. 7 (2024) 618–627.
[63] Z. Yu, S. Li, J. Su, J. Zhang, D. Zhang, Z. Zhou, Z. Qin, X. Liu, Y. Lai, S. Fu, Bio-inspired core-shell structural aerogel with programmable water release capacity for efficient solar thermoelectricity-freshwater cogeneration, Matter 6 (2023) 3509–3525.
[64] M.L. Skoric, I. Lukic, M. Pantic, M.K. Krusic, Z. Novak, S. Milovanovic, Biopolymer aerogels: structural and functional tailoring of starch/sodium alginate networks, Int. J. Biol. Macromol. (2025) 142774.
[65] T. Duong, M. Vivero-Lopez, I. Ardao, C. Alvarez-Lorenzo, A. Forgács, J. Kalmár, C. A. García-González, Alginate aerogels by spray gelation for enhanced pulmonary delivery and solubilization of beclomethasone dipropionate, Chem. Eng. J. (2024) 149849.
[66] B. Ecsédi, A. Forgács, Z. Balogh, I. Fábián, J. Kalmár, Hydration and wetting mechanism of borosilicate–Polyvinyl alcohol (PVA) hybrid aerogels of potential bioactivity, J. Mol. Liq. 401 (2024) 124605.
[67] K. Moldován, A. Forgács, G. Paul, L. Marchese, A. Len, Z. Dudás, S. Kéki, I. Fábián, J. Kalmár, Mechanism of hydration induced stiffening and subsequent plasticization of polyamide aerogel, Adv. Mater. Interfaces 10 (2023) 2300109.
[68] M.Z.I. Khan, D. Rauš̆l, R. Zanoški, S. Zidar, J.H. Mikulčić, L. Krizmanić, M. Eškinja, B. Mildner, Z. Knežević, Classification of loratadine based on the biopharmaceutics drug classification concept and possible in vitro–in vivo correlation, Biologic. Pharmaceutical Bulletin 27 (2004) 1630–1635.
[69] N. Barman, J. Deb, U. Sarkar, Favipiravir drug molecule adsorbed graphyne as a promising drug delivery vehicle for anti-viral treatment, Appl. Surf. Sci. 640 (2023) 158473.
[70] G. Király, J.C. Egu, Z. Hargitai, I. Kovács, I. Fábián, J. Kalmár, G. Szemán-Nagy, Mesoporous aerogel microparticles injected into the abdominal cavity of mice accumulate in parathymic lymph nodes, Int. J. Mol. Sci. 22 (2021) 9756.
[71] P. Herman, A. Kiss, I. Fábián, J. Kalmár, G. Nagy, In situ remediation efficacy of hybrid aerogel adsorbent in model aquatic culture of paramecium caudatum exposed to Hg (II), Chemosphere 275 (2021) 130019.
[72] P. Veres, G. Király, G. Nagy, I. Lázár, I. Fábián, J. Kalmár, Biocompatible silica-gelatin hybrid aerogels covalently labeled with fluorescein, J. Non Cryst. Solids. 473 (2017) 17–25.